THE *EINSTEIN OBSERVATORY* DETECTION OF FAINT X-RAY FLASHES

E. V. GOTTHELF[1]
Laboratory for High Energy Astrophysics, NASA/Goddard Space Flight Center, Greenbelt, MD 20771; gotthelf@gsfc.nasa.gov

T. T. HAMILTON
Department of Astronomy, California Institute of Technology, Pasadena, CA 91125; tth@astro.caltech.edu

AND

D. J. HELFAND
Department of Astronomy and Columbia Astrophysics Laboratory, Columbia University, 538 West 120th Street, New York, NY 10027; djh@carmen.phys.columbia.edu
Received 1995 March 17; accepted 1996 February 8

ABSTRACT

We report on the result of an extensive search for X-ray counterparts to gamma-ray bursts (GRBs) using data acquired with the imaging proportional counter (IPC) on board the *Einstein Observatory*. We examine background sky fields from all pointed observations for short timescale ($\lesssim 10$ s), transient X-ray phenomena not associated a priori with detectable point sources. A total of 1.5×10^7 s of exposure time was searched on arcminute spatial scales down to a limiting sensitivity of 10^{-11} ergs cm^{-2} s^{-1} in the 0.2–3.5 keV IPC band. Forty-two highly significant X-ray flashes (Poisson probability less than 10^{-7} of being produced by statistical fluctuations) are discovered, of which 18 have spectra consistent with an extragalactic origin and light curves similar to the *Ginga*-detected X-ray counterparts to GRBs. Great care is taken to identify and exclude instrumental and observational artifacts; we develop a set of tests to cull events that may be associated with spacecraft or near-Earth space backgrounds. The flashes are found to be distributed isotropically on the sky and have an approximately Euclidean number-size relation. They are not associated with any known sources, and, in particular, they do not correlate with the nearby galaxy distribution. Whether or not these flashes are astrophysical and/or associated with GRBs, the limits imposed by the search described herein produces important constraints on GRB models. In this paper, we discuss possible origins for these flashes; in a companion paper, we use the results of our search to constrain strongly all halo models for GRBs.

Subject headings: gamma rays: bursts — surveys — X-rays: bursts

1. INTRODUCTION

Observational evidence for X-ray counterparts to classical GRBs in the 0.1–100 keV range has been found by several experiments. X-ray bursts in the 6–150 keV band are located to 1° precision with the WATCH all-sky monitor on board the *Granat Observatory* at a rate of ~ 4 yr^{-1} $(4\pi$ sr$)^{-1}$ (Lund, Brandt, & Castro-Tirado 1991). *Ginga* has detected X-ray bursts associated with GRBs in the 1–10 keV band with similar spatial resolution (Yoshida et al. 1989) and has provided evidence for X-ray precursors to GRBs (Murakami et al. 1991). The XMON instrument on the *P78-1* mission also detected coincident X-ray emission in this band (Laros et al. 1984). As with most GRB observations, these experiments, with their broad sky coverage and high background, offer limited spatial resolution and detection sensitivity, leaving open the origin, and thus the nature, of classical GRBs (see Higdon & Lingenfelter 1990 for a pre–*Gamma Ray Observatory* review). The existence of such X-ray counterparts raises the possibility that they could be used to gain more detailed positional information about the associated bursts, constrain models for the burst number as a function of sensitivity, and, of course, constrain directly models of the underlying physical phenomenon. To this end, the imaging X-ray experiment on board the *Einstein Observatory* is ideally suited to search for GRBs with unprecedented sensitivity and spatial resolution.

The *Einstein* IPC operated for 3 yr, producing images of the X-ray sky with arcminute resolution over a 1 deg^2 field of view (FOV). Considering the operating efficiency of the *Einstein Observatory*, this is equivalent to observing the whole sky for 7 minutes. It is therefore not surprising that *Einstein* was not coincidentally pointed at any cataloged GRB that occurred during its mission. However, by searching all images for serendipitous flashes that occurred in portions of the FOV not occupied by any detectable point source, we can locate all transient events with a fluence greater than 10^{-11} ergs cm^{-2}, 3 orders of magnitude lower than the X-ray counterparts of GRBs at the BATSE detection threshold. About 3% of the *Einstein* database was searched previously, and one potentially astronomical event was found (Helfand & Vrtilek 1983); we also find this event in the current search, although we exclude it from our formal sample because it does not meet the stringent background requirements described below. Apart from this pioneering effort, previous standard analysis of these fields used software that was not designed to detect such flashes.

We present the results of our search below. We have found 42 highly significant X-ray flashes. The sky positions of these candidates are not correlated with sources cataloged in the SIMBAD or NED databases, nor are the events found to be coincident in time with known GRBs or solar flares detected by the gamma-ray spectrometer (GRS) aboard the *Solar Maximum Mission* (*SMM*). Most importantly, they are not preferentially found in the direction of nearby galaxies, allowing us to challenge the viability of all

---

[1] Universities Space Research Association.

halo models for GRBs (see Hamilton, Gotthelf, & Helfand 1996).

In § 2, we first present necessary details of the operation of the *Einstein* IPC and the contents of its database; we then describe our search strategy. In § 3, we report the results of the search and examine the temporal, spectral, geographic, celestial, and detector distributions of the flashes, none of which can be used to preclude an astrophysical origin for the events (detailed tests for various nonastrophysical origins are described in Appendix B). In § 4, we evaluate the count rates recorded by the *Einstein* monitor proportional counter (MPC) detector during the IPC flash times. The final section discusses the origin of the flashes that we *do* detect, while our companion paper uses the results of this search to set strong constraints on the origin of GRBs that follow from the flashes we *do not* detect.

2. THE DATA AND THEIR ANALYSIS

2.1. *IPC Instrument*

To fully describe this undertaking, we must first present the workings of the IPC and what is meant by an IPC "count." Details of the *Einstein Observatory* and the IPC can be found in Giacconi et al. (1979) and Gorenstein, Harnden, & Fabricant (1981). A complete description of the types of events that produce detectable counts in the IPC and an analysis of such counts are given in Wu et al. (1991), Wang et al. (1991), and Hamilton & Helfand (1991). We give only a brief introduction here and consider specific relevant issues in later sections.

The *Einstein Observatory* was in service from late 1978 to mid-1981 in an equatorial ($\pm 22°$) low Earth orbit. It carried a high-resolution grazing-incidence X-ray telescope with a 3.4 m focal length and a $\simeq 1° \times 1°$ FOV. The IPC was one of four focal-plane instruments that could be rotated into the optical axis. Simultaneous observations were obtained with an external co-aligned nonimaging monitor counter (§ 4). The IPC was a gas-filled multiwire counter containing an Ar-Xe-CO_2 mixture as the detection medium. The instrument covered an energy range of 0.1 keV $< E <$ 4.5 keV with a resolution of $\Delta E/E \simeq 0.5 E_{keV}^{-1/2}$. The readout system used the "rise time" method to determine event positions to an instrument-limited resolution of from 1′ to 3′ depending on the deposited energy. An anticoincidence guard counter provided on-board real-time hardware rejection of $\gtrsim 99\%$ of the particle background. Particles and cosmic rays that deposited all their energy within the detection volume were rejected by their (slow) time signatures and (extreme) pulse-height signals.

A signal is initiated in the IPC with the introduction of ionizing radiation into the counter gas. X-rays collected and focused by the mirror enter the detection volume through a thin plastic window and interact with the gas via the photoelectric effect. The energy of the resulting primary electron is proportional to the incident photon energy, thus preserving spectral information. As the electron traverses the gas, secondary electrons are generated through collisionally induced ionizations. The resulting electron cloud then drifts through an electric field defined by a set of high-voltage wire planes spaced 3 mm apart. Close to the wires, the electric field strength is high enough (~ 10 kV cm^{-1}) to generate additional collisionally ionized electrons, increasing their numbers exponentially. This charge avalanche lasts a few microseconds and results in a sufficient net elec-

tronic gain to allow a charge pulse, with its distinct rise time signature, to be measured with a charge-sensitive preamplifier. Encoded into the IPC "count" for this interaction is the time, location, and energy of the incident radiation.

The X-rays imaged on the detector included those of Galactic, extragalactic, and solar origin. The diffuse Galactic X-ray background arises from a hot bubble of gas ~ 100 pc in radius that surrounds the Sun (McCammon et al. 1983), a ridge of emission along the Galactic plane (Iwan et al. 1982; Koyama et al. 1986), and a putative corona of hot gas surrounding the Galaxy. The integrated X-ray emission of known active galactic nuclei produces about 40% of the extragalactic X-ray background; the origin of the balance remains unknown. The measurement of these backgrounds by the *Einstein* IPC is discussed extensively in Wu et al. (1991). In addition, the Sun is a copious emitter of X-rays, and, whenever the satellite is illuminated by solar X-rays (a large fraction of the time), a substantial number of X-rays are scattered into the *Einstein* telescope by the residual atmosphere of the Earth (see Wang et al. 1991; Fink, Schmitt, & Harnden 1988 and references therein).

The IPC is also sensitive to non–X-ray events. Low-energy electrons, γ-rays, and cosmic rays initiate avalanche events within the detector. High-energy cosmic rays produce secondary particles and a γ-ray background from spallation in the detector walls, as well as from neutron activation of the spacecraft mass. In addition to this "natural" background, a low-level leak of the on-board Cm/Al fluorescence calibration source produced detectable counts in the higher energy channels (Harnden et al. 1984). Detector anomalies such as a breakdown in the counter gas and electronic malfunctions could also result in recorded counts.

2.2. *IPC Database*

The IPC database consists of 4082 pointed observations comprising 11,230 triplets of data files: XPR, TGR, and ASP. For each detected count, the time-ordered XPR files list an arrival time with 63 μs resolution, raw and gain-corrected (PI) pulse heights digitized in 32 channels, assigned sky and detector positions with 8″ pixel^{-1} binning, and instrument status information. Satellite position and orientation information are given in the ASP files that contain a derived entry for each major frame (40.96 s) and include the Sun's position, the Earth-Sun angle, and the orientation of the satellite with respect to the Earth's magnetic field. Spacecraft and detector status is given in the TGR files, in which an updated record is written each time a status flag or environment code changes. To reject unsuitable time intervals, the IPC data were filtered using the TGR criteria corresponding to standard SAO processing (see Appendix B). This resulted in 184 days of observing time out of a total of 374 days of IPC file time.

2.3. *Search Strategy*

From the filtered data intervals, we extracted 22×10^6 counts distributed among the 11,230 files whose average observing time was ~ 1400 s. Photons recorded in PI bins 2–10, corresponding to a nominal energy range of 0.16–3.5 keV, were used in the search. The mean count rate was $\sim 4 \times 10^{-4}$ counts s^{-1} arcmin^{-2}. We binned the data into spacetime cells 4.3 by 4.3 by 10 s in volume and searched for

cells with 5 or more counts. To exclude all discrete sources, including the bright target object typically found in the center of the FOV, we searched only those spatial cells with a count rate less than 6×10^{-4} counts s^{-1} arcmin^{-2}. Thus, those cells flagged as meeting our criteria contained a minimum flux enhancement of a factor of ~ 50 over the mean rate for that point in space. As a practical matter, all 2179 files with less than 400 s of good time were excluded, since 5 counts in one spatial cell in these short files would exceed our count rate threshold (1084 of these excluded files contained zero events satisfying our data editing criteria). To avoid missing flashes that straddle two cells, we actually binned the data at twice the needed resolution and constructed each search cell from the sum of the eight adjacent (three-dimensional) subcells (i.e., we searched all possible overlapping cells).

A total of 69 events flagged in this way were then inspected for their spatial extent and compared with a simultaneous background count rate defined by a concentric annulus $7'-15'$ in radius and ± 20 s in time of the detection cell (50 s duration).

We rejected all events that represented deviations of less than 3σ above this local background [i.e., in which $3 > |N_{obs} - N_{exp}|/(N_{exp})^{1/2}$, where N_{obs} is the number of counts recorded in the spatial pixel of interest and N_{exp} is the predicted number from the background annulus]. Subsequent scrutiny revealed that the events excluded by this test were associated with satellite sunrise, sunset, or the approach of the South Atlantic Anomaly. Furthermore, in order to exclude events possibly associated with glitches at the beginning or end of an observation interval, we eliminate those occurring within 20 s of gaps in the data. These cuts left a total of 42 accepted events. Formally, we would expect less than one event of such intensity as a result of Poisson noise.

2.4. Detection of X-Ray Flashes

The 42 X-ray flash candidates were analyzed for their spectral and temporal structure. The data constituting an "event" were further characterized in the following manner. The sky position is given by the mean position of all counts falling within $3'$ in space and ± 20 s in time of the three-dimensional detection cell. The event time is taken as the (first) 1 s bin containing the maximum number of counts as determined using a 0.1 s sliding box during the 50 s time window. Each event was then classified based on its time structure as slow or rapid, and based on its spectrum as soft or hard. The rapid events are defined as having more than 4 counts occurring within the 1 s maximum bin defined above. Events for which $N(<1.3 \text{ keV}) < N(\geq 1.3 \text{ keV})$ are defined as hard. The sky position, event times, and characteristics of the events passing the initial inspection are presented in Table 1. Of the 42 events, 36 are slow, 6 are rapid, 18 are hard, and 24 are soft. It is found that all but one of the hard events are slow and that, similarly, all but one of the rapid events are soft. The converse in both cases is not true, however: soft events are both slow (79%) and rapid (21%), and slow events are composed of nearly equal parts hard and soft events.

Light curves are shown in Figure 1 for four representative flashes. The fact that the rise times are shorter than the decay times is not an artifact of our search criteria. In Figure 2, a composite light curve for each temporal class is shown. Each flash has been centered on the 1 s bin with the most counts as described above. Most of the accepted events have a "slow" time structure, with 90% of the counts clustered within a window 15 s in duration compared with 90% window boundaries of 1 s for the rapid events. An aggregate point-spread function (PSF) using all accepted events was produced by centering and stacking events on the computed mean sky positions. The result is plotted in Figure 3 along with the summed spectrum. The resulting PSF resembles a point source, and the summed spectrum, although quite soft, appears astrophysical (see below). The events were then grouped by spectral hardness and analyzed in a similar manner.

Figure 4 displays the PSF and spectra for the soft and hard events separately. The soft events contain on average 11 counts per event and produce a PSF with a normalized radial distribution consistent with a Gaussian of FWHM $\simeq 3'$. This is the signature expected for a point source with the observed soft spectrum imaged by the mirror plus the IPC. The hard events average 7 counts and also produce a radial distribution consistent with an astronomical origin.

In Figure 5, the soft events are compared directly with data from the cataclysmic variable U Gem in outburst, put through the same analysis; it is clear that both the PSF and the spectrum are consistent with those of a real astrophysical source. Figure 6 displays the properties of slow and rapid events separately. The characteristics for the slow events are similar to those of the sample as a whole. The six rapid events contain ~ 16 counts per event for a total of 100 counts and produce a very soft spectrum with 75% of the counts below ~ 0.4 keV. Inspection of the counts contained within those 1 s bins that contained more than 4 counts reveal an even softer spectrum. Recent studies of supersoft objects show that such spectra, although rare, are found in nature (Brown et al. 1994; Greiner, Hasinger, & Kahabka 1991).

A sky exposure map was produced for the complete IPC database by summing up the filtered time intervals for each sky pointing. The map is plotted in Galactic coordinates in Figure 7 with the candidate flash locations overlaid. The accepted events are roughly isotropic on the celestial sphere. In particular, as we show in the accompanying paper (Hamilton et al. 1996), they are not found preferentially in the direction of nearby galaxies.

A log N–log S curve for all accepted events was constructed using a mean conversion factor of 2.6×10^{-11} ergs cm^{-2} counts^{-1}. We compensated for the off-axis mirror reflection efficiency using the standard IPC vignetting correction (Harris & Irwin 1984, chap. 5, p. 18). The result is plotted in Figure 8 along with various GRB measurements (Hingdon & Lingenfelter 1990). Although it is quite possible that both the γ-ray and the X-ray event curves suffer from instrumental bias (see Higdon & Lingenfelter 1984 and Mazets & Golenetskii 1987 for a review of this issue as related to the Konus data, and Meegan 1994 for a discussion of the BATSE results), a simple straight line between the two curves gives a differential slope of ~ -1.7, similar to the slope detected by BATSE for the number-size relationship of the faintest bursts it detects and considerably flatter than the ~ -2.5 slope for a homogeneous Euclidean distribution.

As discussed above, the flashes exhibit a variety of temporal and spectral characteristics. These effects are not uncorrelated, the softest flashes often having the fastest rise times.

TABLE 1

List of Faint IPC Flashes

Event Time (UT)	R.A. (B1950)	decl. (B1950)	Spectral Hardness[a]	Temporal Structure[a]	Offset Angle[b]
01/12/79 05:32:45......	00ʰ44ᵐ51ˢ	41°46'20"	Soft	Slow	27'
01/22/79 10:57:34......	14 59 38	21 25 29	Soft	Slow	33
01/24/79 00:40:21......	13 52 43	05 35 03	Soft	Slow	31
02/26/79 12:05:12......	04 05 45	−72 04 13	Hard	Slow	42
04/10/79 17:23:16......	05 25 35	−70 47 55	Soft	Slow	33
05/25/79 21:09:21......	23 02 54	−23 21 53	Hard	Slow	44
08/03/79 23:25:48......	03 17 25	42 12 18	Hard	Slow	42
08/13/79 20:19:00......	15 42 20	21 01 42	Soft	Rapid	39
08/29/79 05:51:29......	23 58 22	79 11 19	Hard	Slow	45
08/29/79 15:40:52......	16 00 41	15 28 08	Hard	Slow	36
10/04/79 23:41:55......	05 40 53	49 28 13	Soft	Rapid	30
10/06/79 21:22:56......	19 32 51	21 28 49	Soft	Rapid	39
10/19/79 23:56:37......	06 00 41	−40 09 24	Hard	Slow	18
10/26/79 14:25:16......	09 06 15	17 00 04	Soft	Rapid	36
11/07/79 19:55:45......	06 27 11	−55 18 04	Hard	Slow	17
11/22/79 10:32:38......	20 47 40	29 10 41	Hard	Slow	26
11/25/79 17:11:26......	20 10 32	36 45 58	Soft	Slow	44
12/03/79 04:04:49......	10 46 21	09 10 06	Hard	Slow	38
12/05/79 17:40:11......	12 11 07	14 25 33	Hard	Slow	32
12/15/79 10:16:33......	23 46 40	−28 22 23	Hard	Rapid	39
12/16/79 15:25:51......	12 16 42	30 12 37	Soft	Slow	16
01/17/80 05:59:19......	02 36 16	−08 43 57	Soft	Slow	37
01/17/80 05:57:09......	02 35 42	−08 24 44	Soft	Slow	43
02/05/80 13:28:17......	12 05 23	−52 42 58	Soft	Slow	34
02/12/80 15:15:56......	15 50 29	−23 22 25	Soft	Slow	31
03/25/80 20:00:19......	06 40 06	09 59 26	Soft	Slow	32
04/09/80 14:17:18......	07 37 36	18 01 48	Soft	Slow	36
04/13/80 20:36:16......	05 00 39	−69 35 37	Soft	Slow	39
04/14/80 01:37:18......	19 20 41	−00 13 45	Hard	Slow	32
04/14/80 10:34:24......	17 02 13	60 56 24	Soft	Slow	15
04/16/80 11:26:08......	00 50 10	−72 59 20	Soft	Slow	32
07/08/80 03:16:11......	12 33 13	15 50 19	Soft	Slow	33
07/08/80 05:18:58......	14 13 36	00 54 38	Hard	Slow	37
07/12/80 14:27:10......	13 07 06	−00 53 22	Hard	Slow	28
08/07/80 22:18:57......	15 27 02	12 09 49	Hard	Slow	33
08/20/80 20:56:42......	16 03 19	18 42 30	Soft	Slow	22
08/20/80 21:56:08......	16 01 05	18 13 11	Soft	Rapid	37
03/01/81 07:29:46......	18 41 48	20 06 05	Soft	Slow	34
03/18/81 06:23:56......	04 46 11	11 10 15	Hard	Slow	7
04/01/81 18:21:48......	17 32 15	−12 35 03	Soft	Slow	41
04/03/81 16:54:50......	17 33 46	−08 13 33	Hard	Slow	31
04/25/81 14:56:47......	09 27 44	06 00 05	Hard	Slow	30

[a] See § 3 for definitions.
[b] Distance of the flash from the detector center.

Although all 42 flashes taken together do not show any correlation with position in the detector, when we examine only the soft-rapid flashes, we find that their positions in physical detector coordinates are preferentially aligned along the directions of the counter wires. While it is by no means excluded that some regions of the counter may have heightened sensitivity to genuine astronomical events, the observed pattern suggests that these events may originate within the detector. One possible explanation is that these events are afterpulses, counter events that result when not all of the electrons from a rejected particle event fall within the effective counter dead time; i.e., one or a few slow-moving electrons may not have reached the counter wires until after the counter has reset following the event which generated them. These events have been well studied in the *ROSAT* PSPC (Snowden et al. 1994), and it is very unlikely that groups of afterpulses would appear as discrete counts, as do the events that make up the flashes (S. Snowden 1994, private communication). However, we consider it likely that the softer and/or more rapid flashes detected by our search are related to afterpulses or some other counter phenome-

non, and we excluded them from further consideration. The fact that we thereby delete 24 events as possible counter artifacts does not imply that we necessarily believe the remaining 18 events with slower rise times and harder spectra to be true astronomical events.

3. MPC RESULTS

The *Einstein* MPC was an independent nonfocal plane instrument co-aligned with the optical axis of the *Einstein Observatory*. The MPC was a collimated proportional counter with a 1.5 mil beryllium window that was sensitive to 1–20 keV X-rays. During normal operation, the MPC simultaneously observed the entire FOV being observed by the IPC. Thus, while the flashes we observe with the IPC may, if they have a hard spectrum, be observable with the MPC, the thousandfold increase in effective background in the MPC would make detection of transients at these flux levels impossible. However, by summing the MPC data for the 18 hard flashes we detect, we may test whether the events are astronomical and also constrain their spectrum.

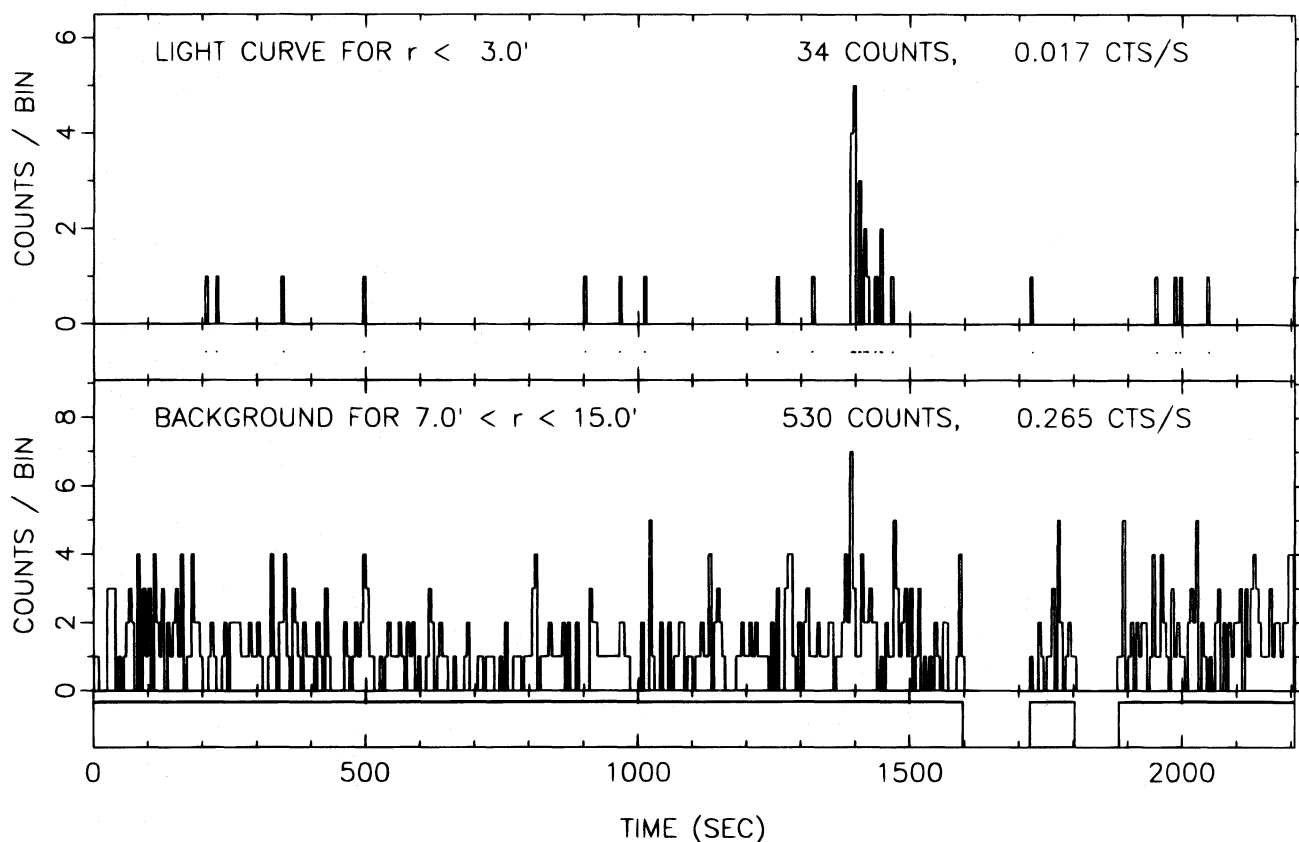MPC data readily available from the High-Energy Astro-

LIGHT CURVE FOR r < 3.0'   34 COUNTS,   0.017 CTS/S

BACKGROUND FOR 7.0' < r < 15.0'   530 COUNTS,   0.265 CTS/S

TIME (SEC)

FIG. 1a

LIGHT CURVE FOR r < 3.0'   46 COUNTS,   0.020 CTS/S

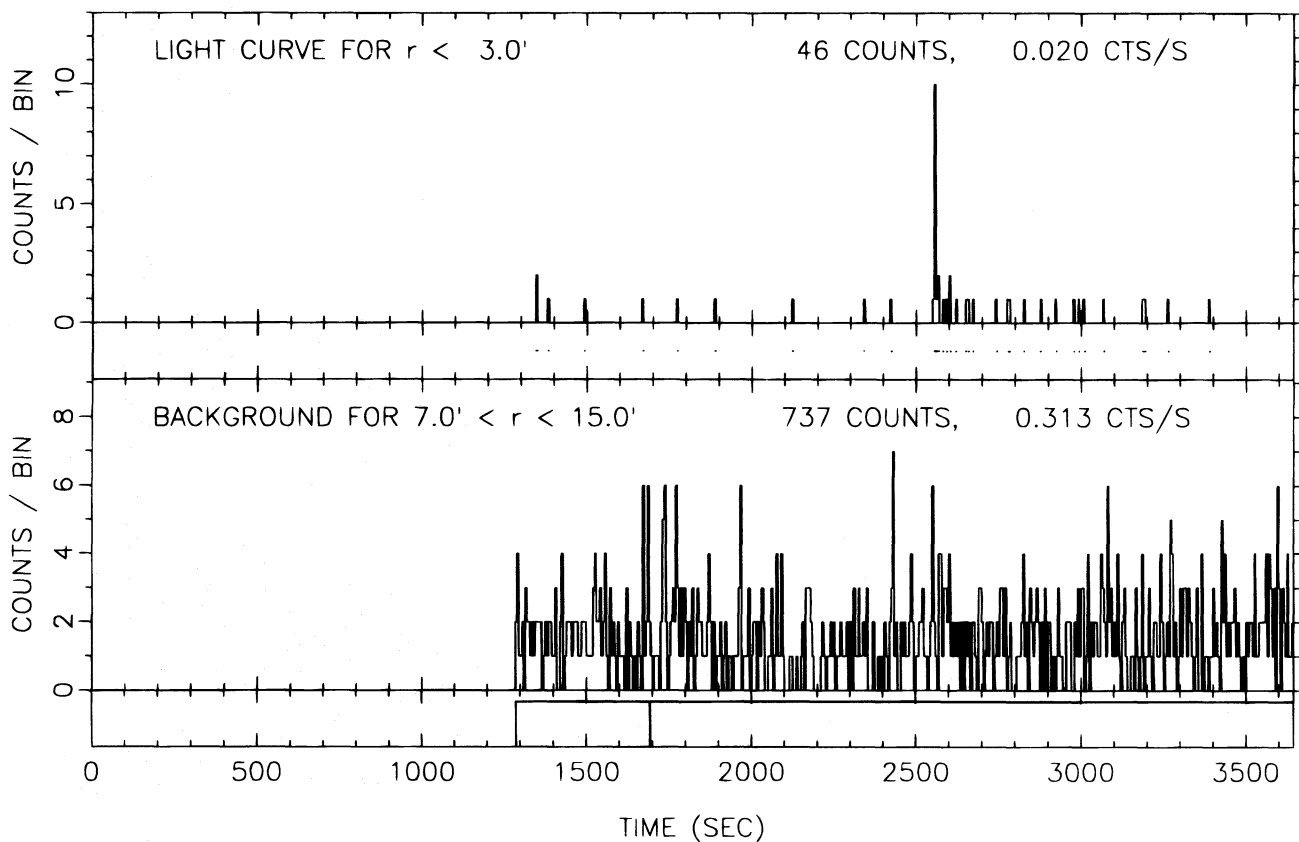BACKGROUND FOR 7.0' < r < 15.0'   737 COUNTS,   0.313 CTS/S

TIME (SEC)

FIG. 1b

FIG. 1.—Light curves for four typical flash events. The flashes in (a) and (b) are categorized as slow, and those in (c) and (d) as rapid. The central strip in each plot shows the arrival times of the photons as dots. The bottom strip shows the times of housekeeping status changes as vertical lines. This indicates that the flashes are not associated with detectable changes in the state of spacecraft or instrument.

LIGHT CURVE FOR r < 3.0'   31 COUNTS,   0.015 CTS/S

BACKGROUND FOR 7.0' < r < 15.0'   438 COUNTS,   0.210 CTS/S

TIME (SEC)

Fig. 1c

LIGHT CURVE FOR r < 3.0'   9 COUNTS,   0.006 CTS/S

BACKGROUND FOR 7.0' < r < 15.0'   404 COUNTS,   0.254 CTS/S
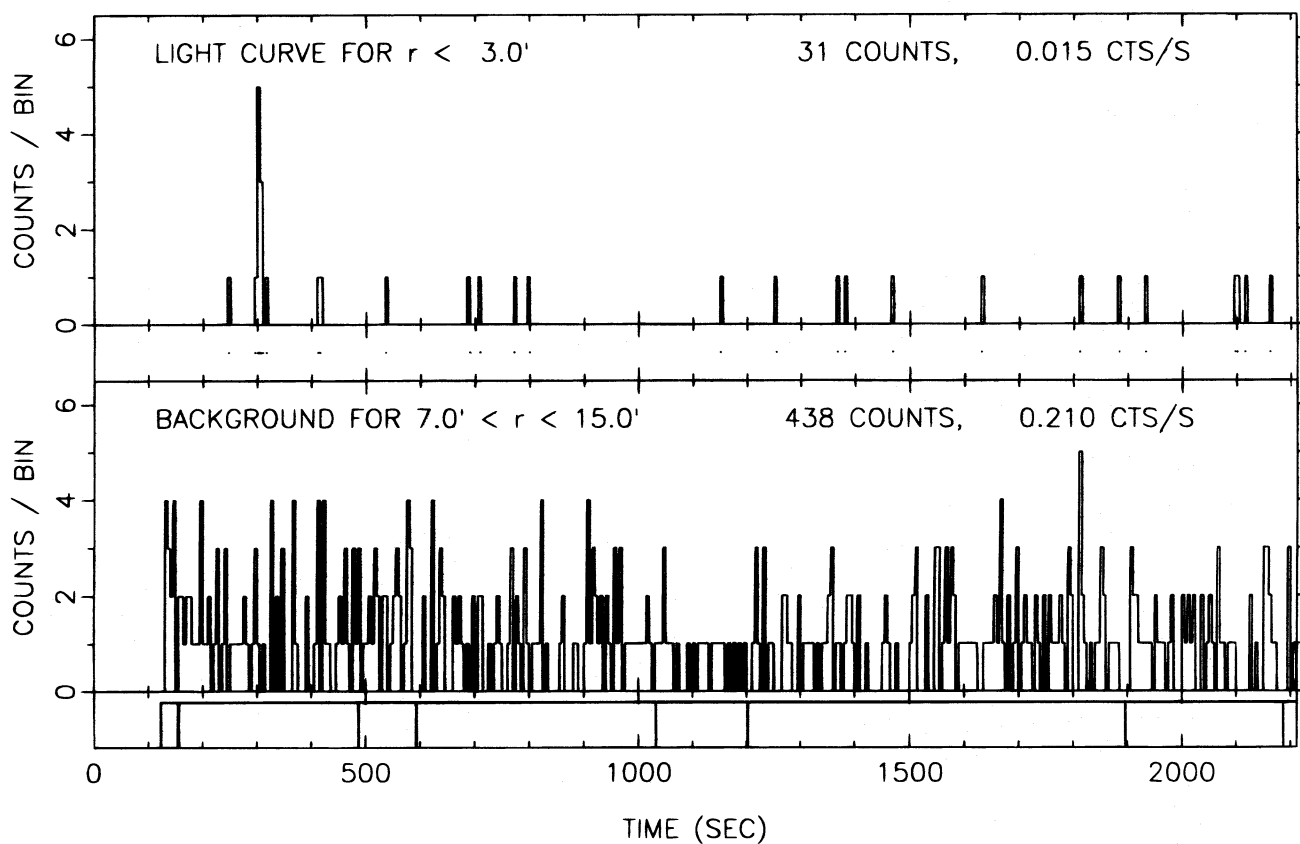
TIME (SEC)
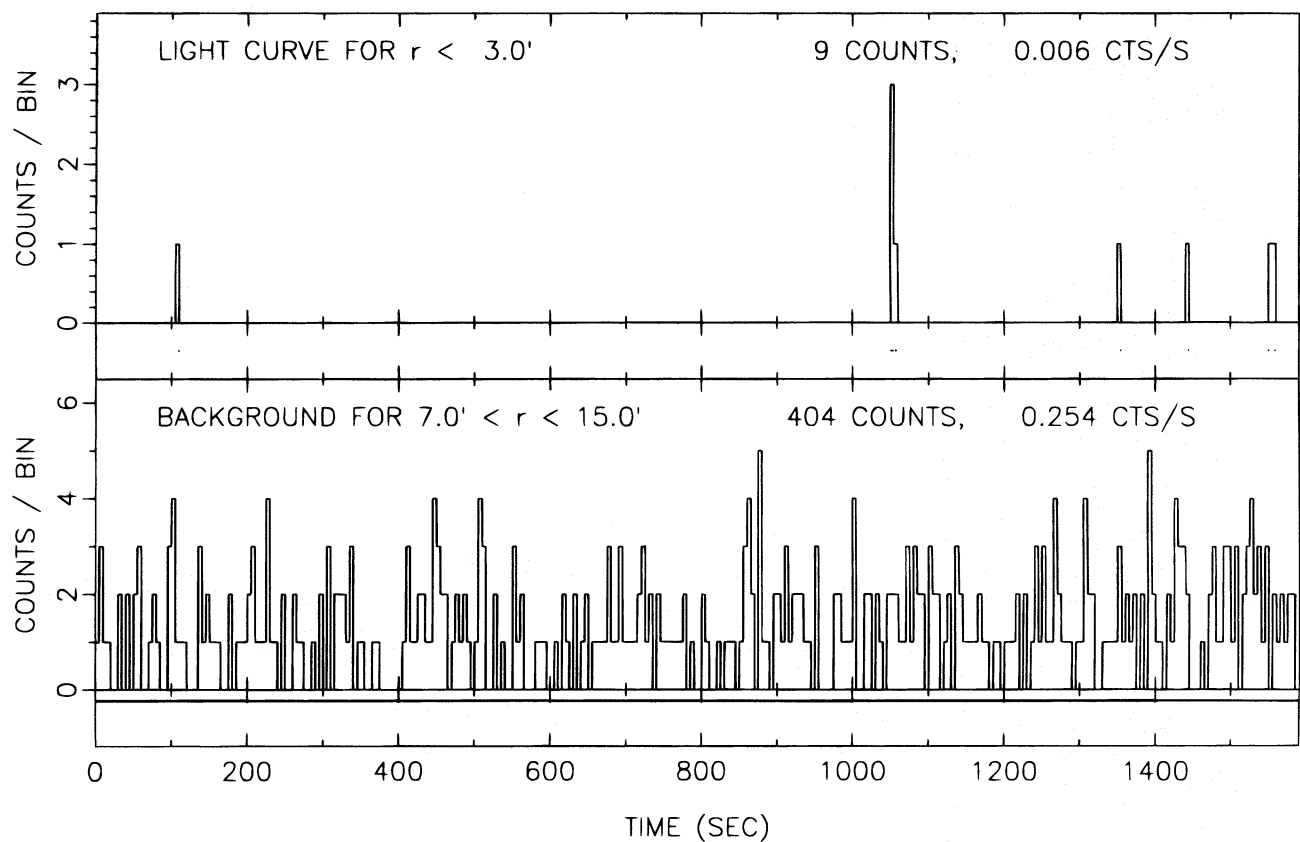
Fig. 1d
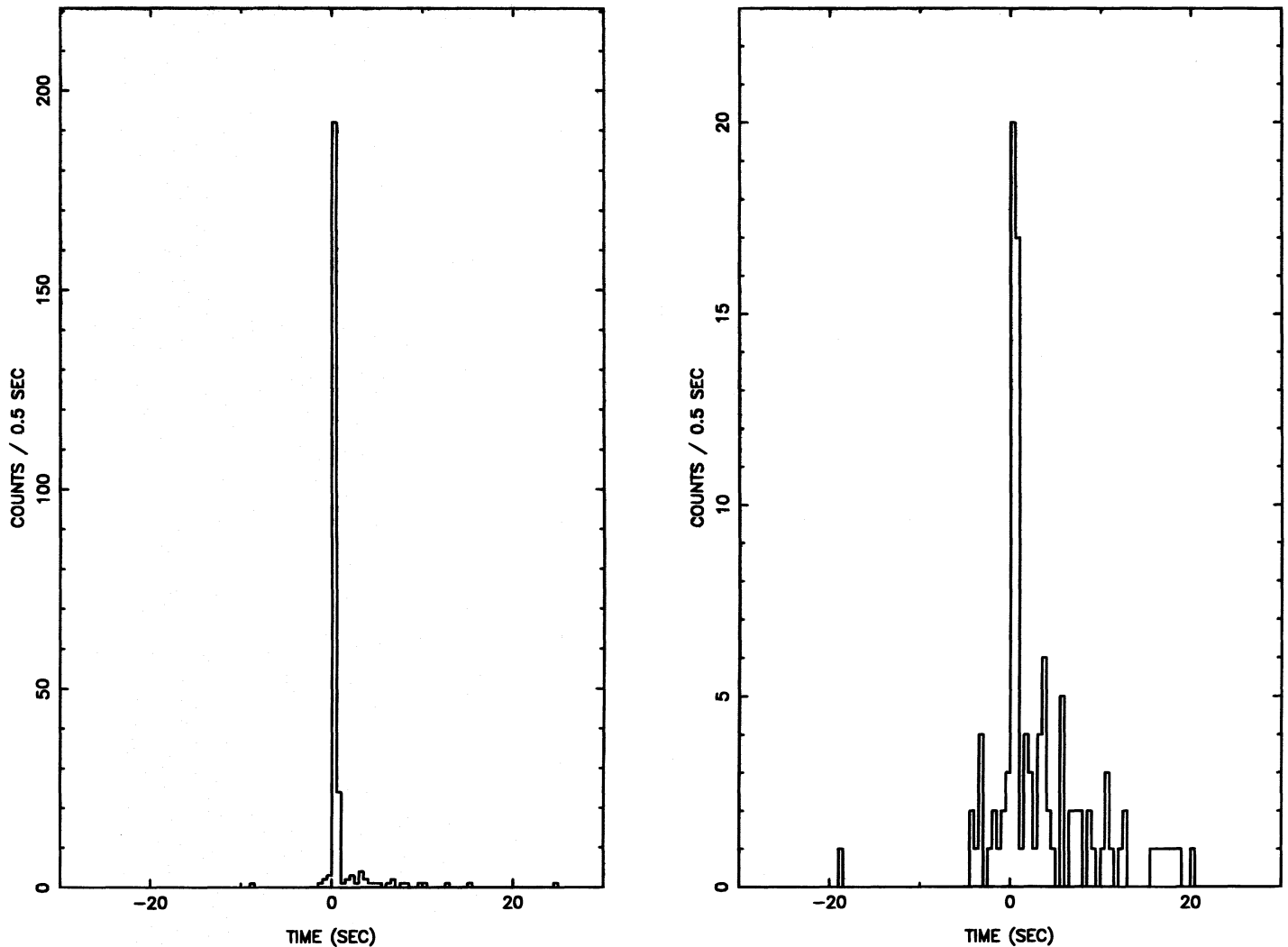
Fig. 2.—Composite light curves for the X-ray flashes are shown for both slow (*right*) and rapid (*left*) events. Both curves show a rise time significantly shorter than the decay time. Since our search method is symmetric with respect to time, this asymmetry is a real effect.

physics Science Archive Research Center (HEASARC) at Goddard Space Flight Center report the total MPC counts in 2.6 s bins. A typical bin in a field with no bright sources, such as those examined in our IPC investigation, contains about 40 counts. We compared the counts in the time bin in which we detect flashes to an expected background equal to the mean of the four preceding and four following bins. Of the 18 hard events, which one might reasonably expect to have MPC counterparts, three had no MPC data, one came at the first bin of an MPC observation, and one corresponded to a mean MPC rate of over 100 counts s^{-1}. Excluding those five events leaves 13 hard events with good MPC data. The mean MPC rate was 45, the extremes 64 and 37. None of the MPC intervals corresponded to a count rate excursion of more than 14, or about 2 σ. In four of the intervals, the count rate at the time of the flash was less than or equal to the expected background. In 10 of the intervals, the count rate was higher. The total count in the thirteen 2.6 s bins corresponding to the flash peaks was 647. This is 2.5 σ above the expected background of 587. This is encouraging but hardly a definitive confirmation of an astronomical origin for the flashes.

The mean fluence per MPC flash is therefore 4.6 photons, although this number is probably an underestimate of the true fluence as a result of the restrictive time bin used here. If the MPC events had the same time signature as the IPC flashes, our procedure would detect about half of the total fluence. The hard IPC flashes themselves have a mean fluence of 7 photons. The ratio between MPC and IPC is consistent with a 1.7 keV thermal plasma or a power law with a photon index of 2. This is reasonably near the observed *Ginga* GRB X-ray spectrum.

3.1. *Discussion*

Our search for X-ray transients found a total of 42 in the *Einstein* database. This result is a robust upper limit on transient X-ray phenomena at the detected flux levels. However, the origin of the signals that we do detect remains a mystery. While we have been unable to provide a definitive explanation, several possibilities are evident. The least interesting is that the flashes are a result of some hitherto unknown phenomenon that takes place entirely within the detector. As discussed above, it may be that many (or even all) of the flashes are the result of a phenomenon analogous to the afterpulses detected in *ROSAT* (Snowden et al. 1994). Of course, it is unlikely that such a phenomenon would manifest itself with a point response function and spectrum that perversely imitate incident cosmic X-rays, but this
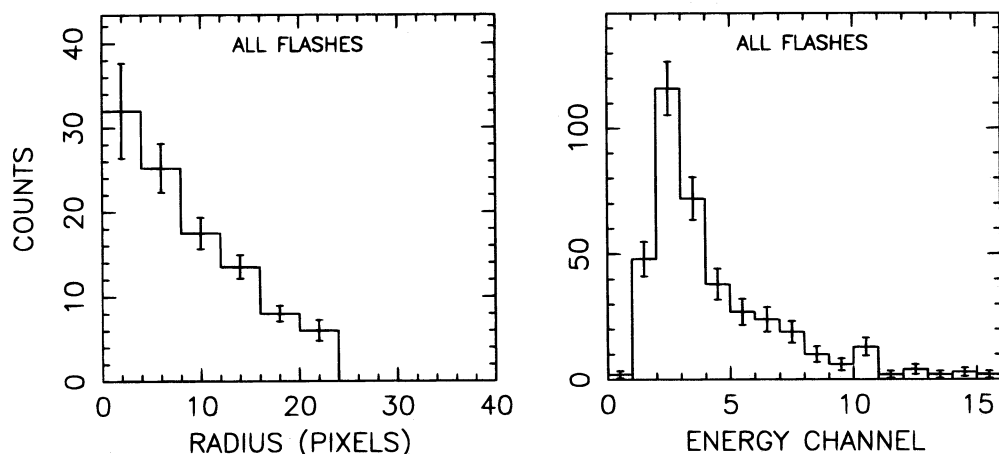
FIG. 3.—Composite radial distribution and spectrum for the 42 flashes. One pixel is 8″. The radial distribution is consistent with the point response function of the IPC.
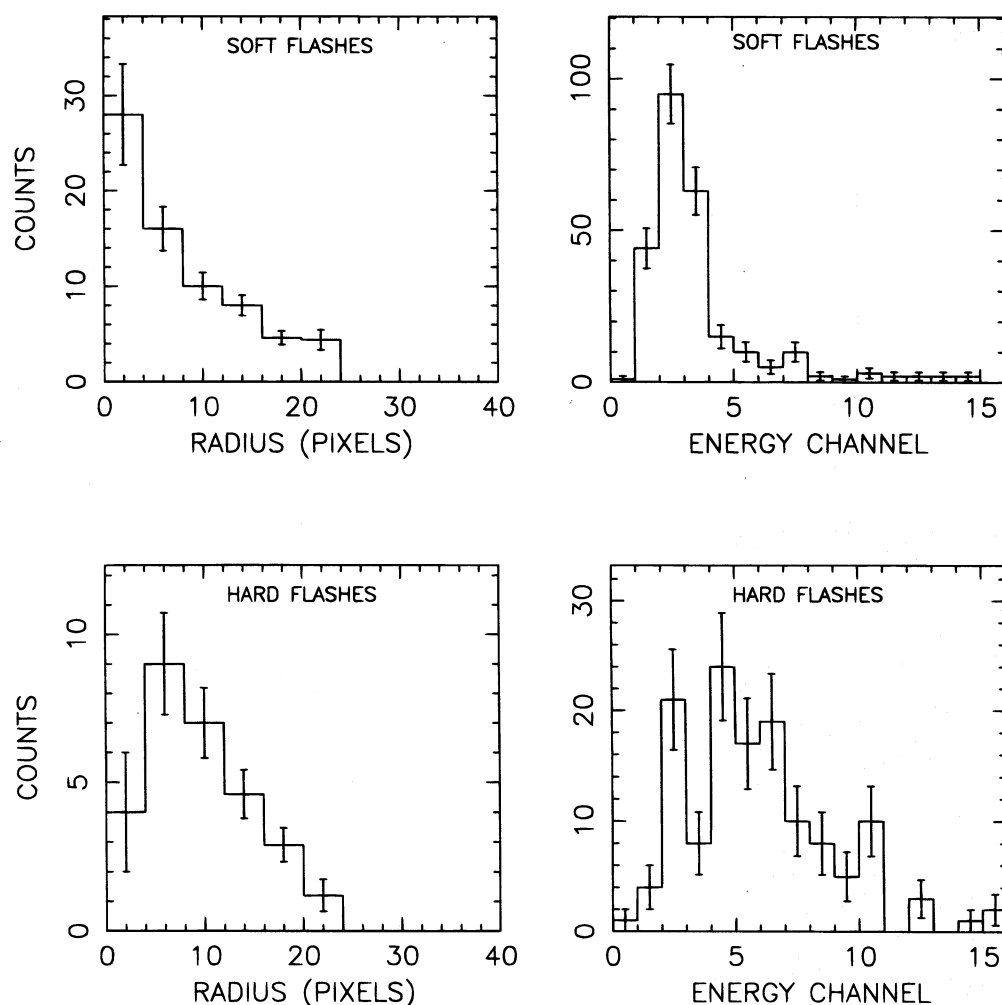

FIG. 4.—Composite radial distribution and spectrum for each spectral classification. Both radial distributions are consistent with a point source origin.

possibility cannot be excluded. A second obvious explanation is that the flashes originate outside the spacecraft but within the solar system. The fact that the flashes do not correlate with solar-related phenomena such as the illumination of the spacecraft by the Sun discourages, but does not refute, such an explanation. We have performed a number of tests to determine if the flashes correlate with any nonastronomical phenomenon. The tests are described in Appendix A. We conclude from these tests that an astronomical origin for the flashes cannot be ruled out. Indeed, some of the properties of the flashes support particular types of astronomical interpretations.

The isotropic distribution of flashes on the celestial sphere indicates that they originate at distances either large or small compared with the length scale of the Galaxy (~ 10 kpc). The homogeneous differential slope of -2.5 exhibited
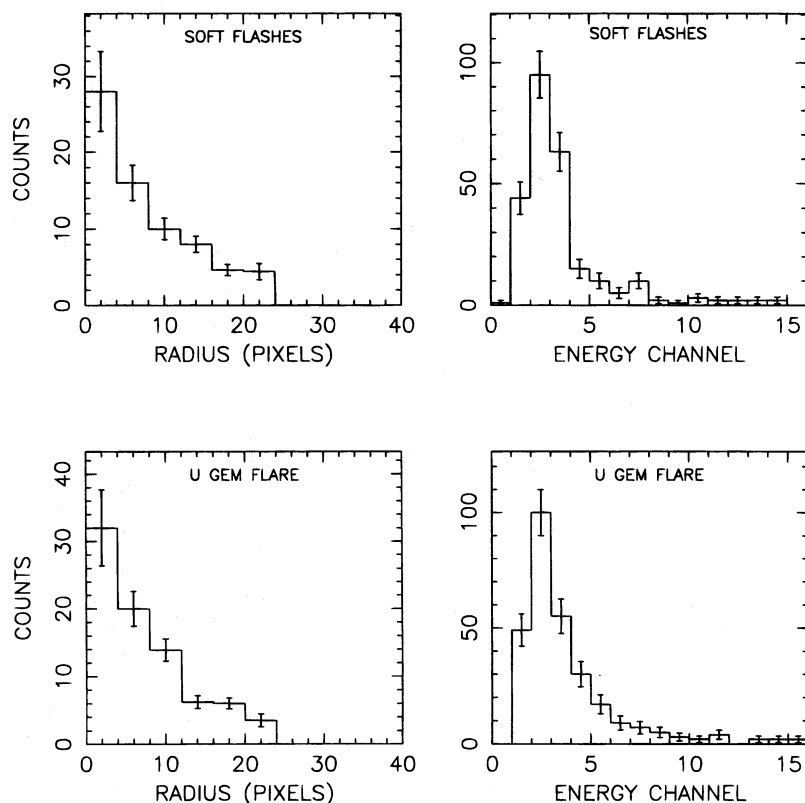
FIG. 5.—Comparison of the composite radial distribution and spectrum of the soft flashes and that of U Gem in outburst analyzed in the same manner. The U Gem outburst was one of the softest celestial sources detected by the IPC. This plot contains 200 s of data from the HUT 1474851 + 4100. The similarity of the spectra demonstrates that, although the soft flashes do have an extremely soft spectrum, it is a spectrum consistent with a celestial origin of the photons.
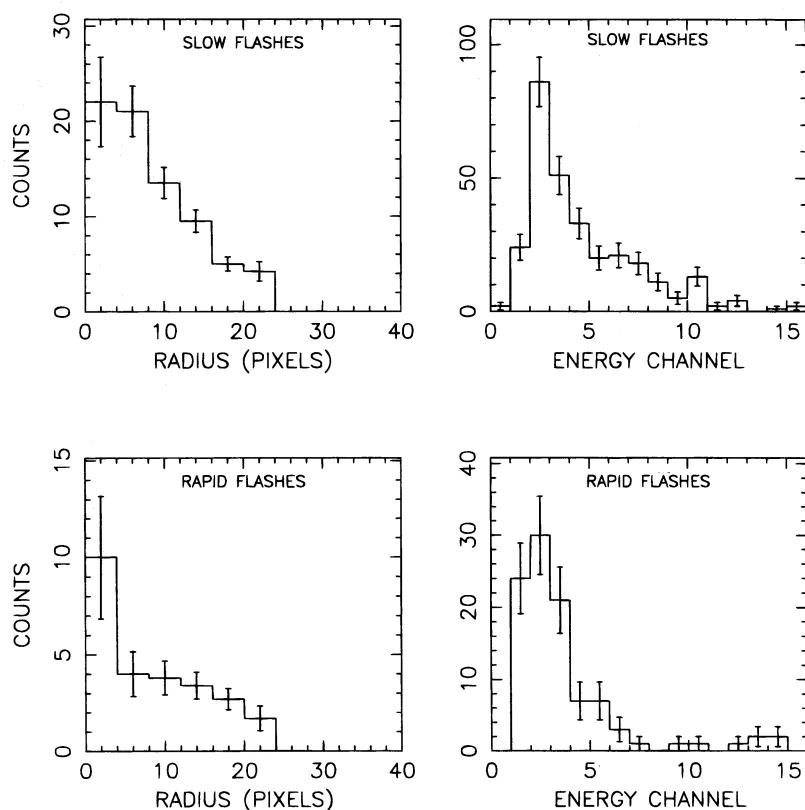

FIG. 6.—Composite radial distributions and spectra sorted by temporal class. In the bottom two panels, only events occurring in the brightest 1 s of the rapid flashes are included.
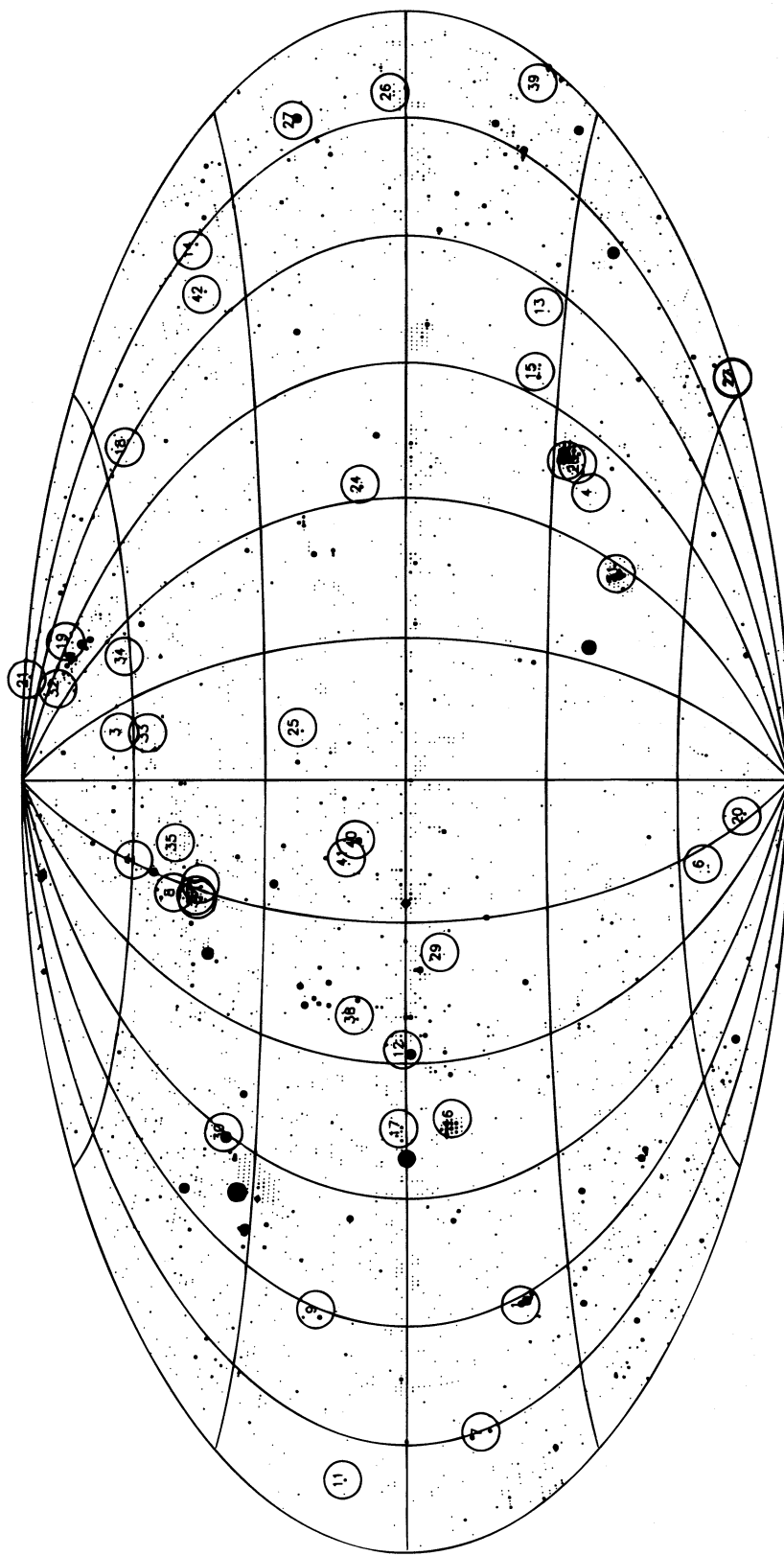
FIG. 7.—Location on the celestial sphere of the 42 X-ray flashes overlaid on an IPC sky exposure map. The symbol size for each exposure is proportional to the duration of the exposure. The flashes are clustered in areas of the sky, such as the LMC, which were observed for long periods. The density of flashes per unit exposure time does not correlate with Galactic latitude or the locations of any known class of object.

by the flash log N–log S relation is consistent with either an extragalactic or a local origin for the flashes. While the time structure, space distribution, and apparent luminosity function of the X-ray flashes is reminiscent of GRBs, the fluence of the observed flashes is several orders of magnitude fainter. If the flashes originate at a distance of 1 pc, the required energy is $\sim 10^{28}$ ergs, equivalent to the energy released by the accretion of $\sim 10^9$ g of material onto a compact object. If the flashes originate at 1 Gpc, then a typical energy would be $\sim 10^{46}$ ergs.

Although our experiment is sensitive to flashes on a timescale of up to ~ 10 s, the flashes we detect characteristically have a substantially shorter timescale; indeed, the flashes have a timescale shorter than the X-ray counterparts of GRBs detected by *Ginga*, especially if one postulates an origin at cosmological distances that would require substantial time dilation in the faintest (most distant) bursts. They are not obviously shorter than the X-ray timescale of the soft gamma repeaters (SGRs) detected by the *Advanced Satellite for Cosmology and Astrophysics* (*ASCA*), although the X-ray light curve of the *ASCA* SGR is not well constrained because the *ASCA* gas scintillators saturated their telemetry buffer after only five events (Murakami et al. 1994). We note, however, that the flashes we detect cannot be counterparts to cosmological GRBs if the latter are standard candles, since, for a faint BATSE burst redshift of ~ 1–2, there is insufficient volume of universe at greater distances to produce events 30 times fainter with the frequency we observe.

The flashes are also far more numerous than known GRBs: we observe a rate of 2×10^6 yr^{-1} over the whole sky. This is approximately the frequency with which supernovae occur within 1 Gpc, which prompts the speculation that the X-ray flashes are produced by the breakout of supernova shocks as they reach the optically thin regions of exploding stars. This would require the release of $\sim 10^{-7}$ of the supernova's energy in a prompt ultraviolet/soft X-ray flash. It is clear, however, that not all of the observed flashes originate beyond the Galaxy, since one soft event occurs at a Galactic latitude of 2°.

The isotropic nature of the flashes' distribution is of course consistent with an origin relatively nearby in the Galaxy. It is tempting to propose as progenitors local flare stars and/or RS CVn systems. The soft spectra of the detected flashes indeed suggest a coronally active star population. Given the flare frequency and duration of a typical flare star, there is a reasonable chance to catch a flare event during a typical IPC observation. But, again, the number of flashes is inconsistent with local field star densities. Perhaps the flashes are associated with a Galactic population of old, isolated neutron stars that is otherwise invisible.

Of course, there is no reason to believe that the 42 events we have detected, or even the 18 with harder spectra and slow timescales, have a common origin. They may represent a maddening combination of interesting astronomical events and indistinguishable counter artifacts. In any case, the observed flash rate is a definite upper limit on the occurrence of faint astronomical X-ray transients. The significance of this limit as related to GRBs is explored in Hamilton et al. (1996).

APPENDIX A

TESTS FOR A NONASTROPHYSICAL ORIGIN OF THE IPC FLASHES

In order to determine if the detected flashes truly have an astrophysical origin, we devised a series of tests based on coverage and sensitivity arguments.

One possible nonastrophysical origin for the observed flashes is arcing associated with a particular spot on a counter wire. If this were the cause of our events, the point response function should differ significantly from that observed for real celestial sources. Our search box is much larger than the IPC point response function (18 vs. $\lesssim 7$ arcmin^2), so a statistical noise fluctuation would also look very different. In addition, the spectrum from instrumental artifacts would not show the familiar effects of counter window absorption (mainly carbon at 0.28 keV). As mentioned in § 3, the PSF resembles a point source, and the spectrum appears astrophysical.

The gain and other counter properties varied substantially during the life of the satellite, so we knew that, if occurrence of transients was concentrated in one part of the mission, the cause was probably instrumental. Thus, we plotted the time of occurrence for events during the mission. The result is shown in Figure 9 along with the daily fraction of filtered IPC time coverage (total time intervals passing the standard processing criteria per day). A Kolmogorov-Smirnov (K-S) test yields a probability of 78% that the distribution is random with respect to spacecraft lifetime (Fig. 10). We also calculated the distribution of events with respect to local solar time. The total filtered IPC observing time was binned into hourly intervals and compared with the event distribution. An excess of occurrences on the leading side of the Earth's orbital motion would suggest X-rays from meteoritic material interacting with the Earth's atmosphere. No such effect is seen (Fig. 11).

Nuclear reactors aboard Soviet spy satellites are a potential source of nonastrophysical γ-ray and X-ray transients. Recently, declassified results from the *SMM* GRS experiment have detailed the cause and properties of these events (Rieger et al. 1989; Share et al. 1989; Hones & Higbie 1989; O'Neill et al. 1989). *SMM* and *Einstein* flew concurrently and in similar orbits for about a year from 1980 February 14 onward. During the overlap of the two missions, an average of three anomalous events per month were detected by *SMM*. We compared the monthly event rates given by Rieger et al. (1989; see Fig. 12) with that of our flashes (normalizing by coverage) and do not see a significant correlation. However, this is not a strong test because the data set is too sparse, and the rate is dependent on altitude and orbit. We looked for a periodic recurrence rate relative to the *Einstein* orbit by plotting the time of day of the flash occurrence against day number (see Rieger et al. 1989). Again no obvious trend is evident.
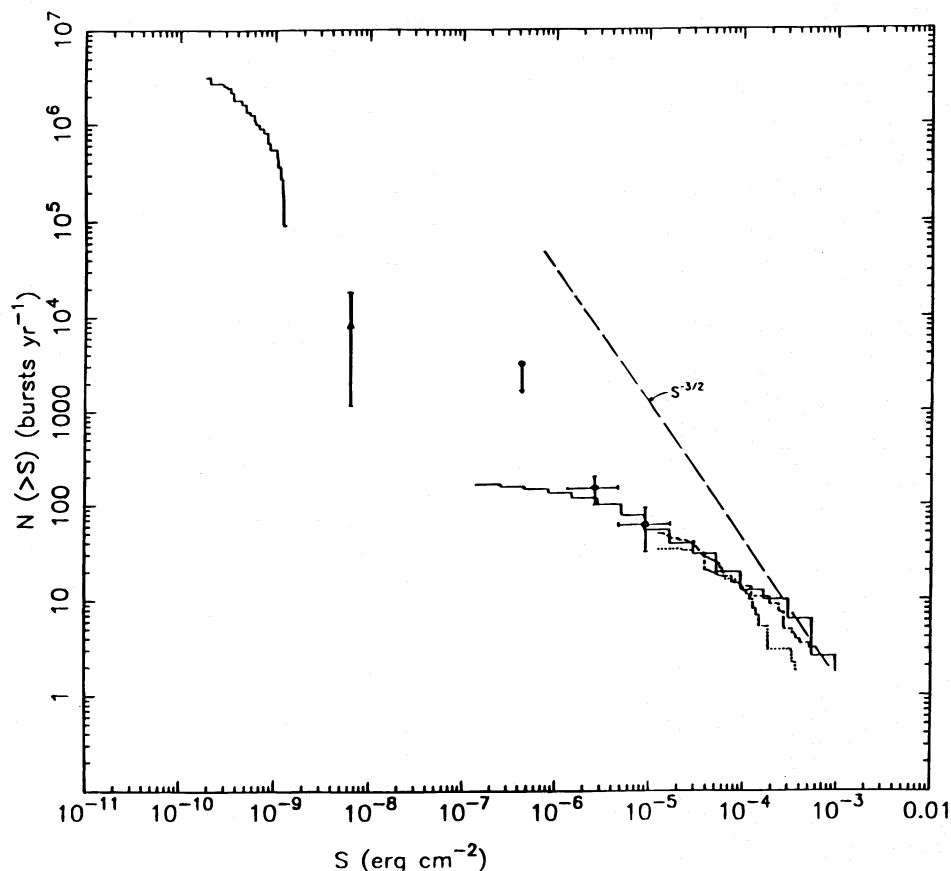
FIG. 8.—The log N–log S relationship for the X-ray flash fluxes reported in this paper plotted along with the log N–log S relations found by various GRB experiments (see Fig. 6, Hingon & Lingenfelter 1990).

The ASP file data, filtered with the TGR data, were used to construct a satellite Earth coverage map. The geographic location of the satellite at the time of the events is shown in Figure 12. The shading represents the time that the satellite spent operating at the designated latitude and longitude, e.g., the unshaded area in the southern hemisphere corresponds to the South Atlantic Anomaly. No correlation with latitude or with putative nuclear test sites is found.

A detector exposure map was made for our flash search by summing the filtered times passing both the maximum count rate criteria and the minimum count criteria as a function of detector coordinates (Fig. 13). As expected, the exposure in the center of the counter is suppressed because of the presence of target sources in the field. The outline of the window support ribs is also apparent and is due to two competing effects. Because of the geometric blockage of the various X-ray background contributions, the low count rate exposure is enhanced under the ribs, but the chance of falling below the minimum count threshold is increased and thus the exposure is decreased overall. The region with the most exposure lies just outside the ribs, where vignetting decreases the background count rate and increases the sensitivity of our search.

We plotted the flashes in detector coordinates and found a generally smooth distribution with an enhancement toward the edge of the field (Fig. 14). This is consistent with our exposure map. In Figure 14, we outline the location of the window support ribs and the nominal window edge. The size of the ribs is energy dependent, so that a flash can appear to be " under " the rib, particularly since the PSF is relatively broad at low energies. We used a definition for the rib width of 4.'3. Our detector exposure map includes all the available area, including the area outside that used in the standard SAO processing, where the quality of the detector linearization, thus the aspecting, is rather poor. Thus, two flashes appear to be just outside the detector window. However, again, this is consistent with the exposure.

To test this qualitative impression of consistency, we created a histogram of exposure time intervals and calculated the number of flashes expected in each based on the total number of flashes observed. The expected and actual distributions based on the exposure time accumulated at various points on the detector were consistent at the 66% confidence level (χ^2 value of 10.4 for 13 degrees of freedom).

Our somewhat disappointing conclusion after this evaluation is that the possibility that the transient events are of astrophysical origin cannot be established or excluded. If they are celestial events, their isotropy is consistent with an origin at the sites of the GRBs; however, other possibilities, such as origins at sites in the Oort cloud or a local Galactic population, cannot be excluded. An expanded version of this discussion may be found in Gotthelf (1992).
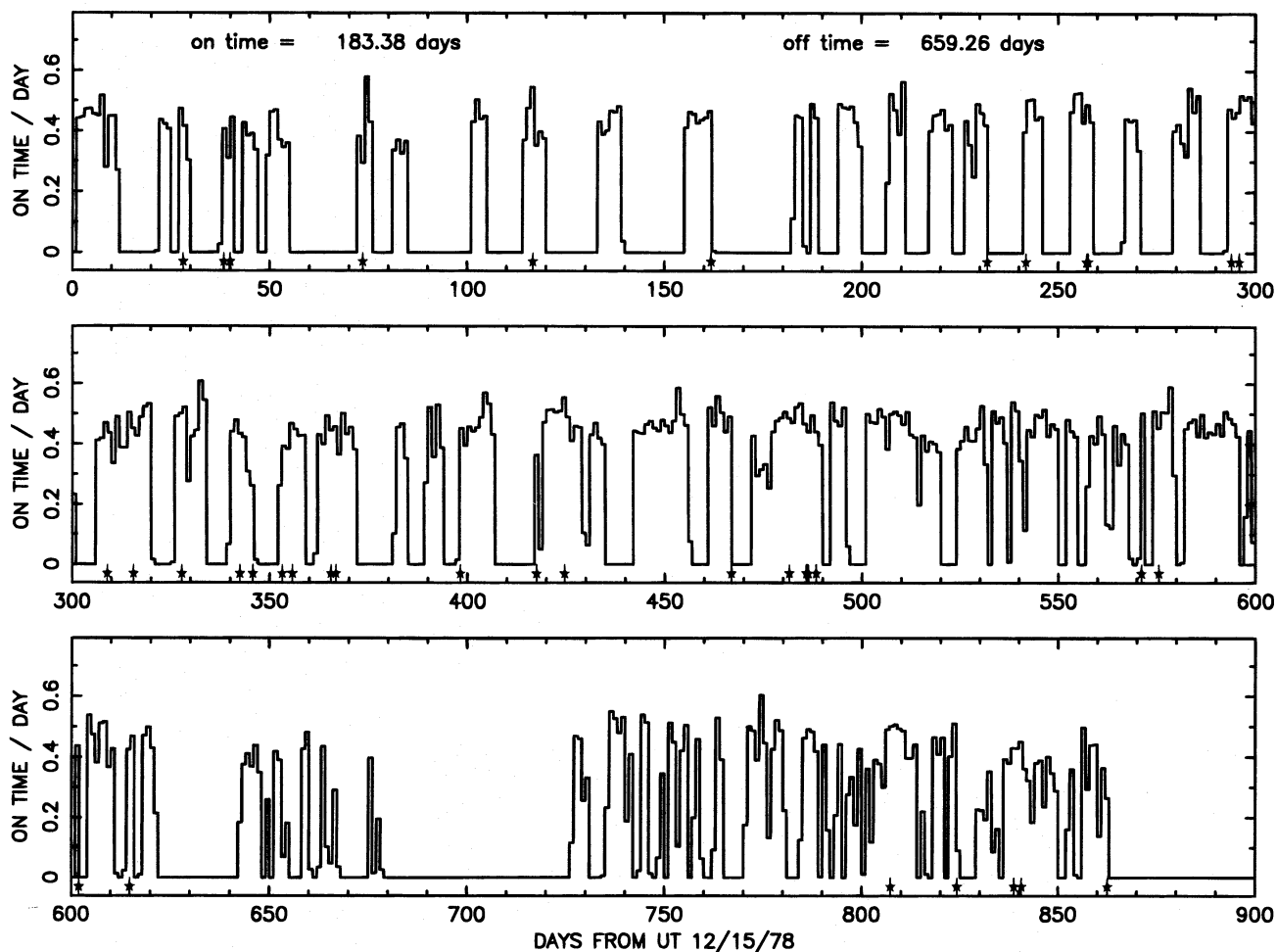
on time = 183.38 days off time = 659.26 days

Fig. 9.—Daily IPC time coverage, including only the time intervals passing the standard processing criteria (see Table 2). The times of occurrence of the 42 flashes are indicated along the abscissa.
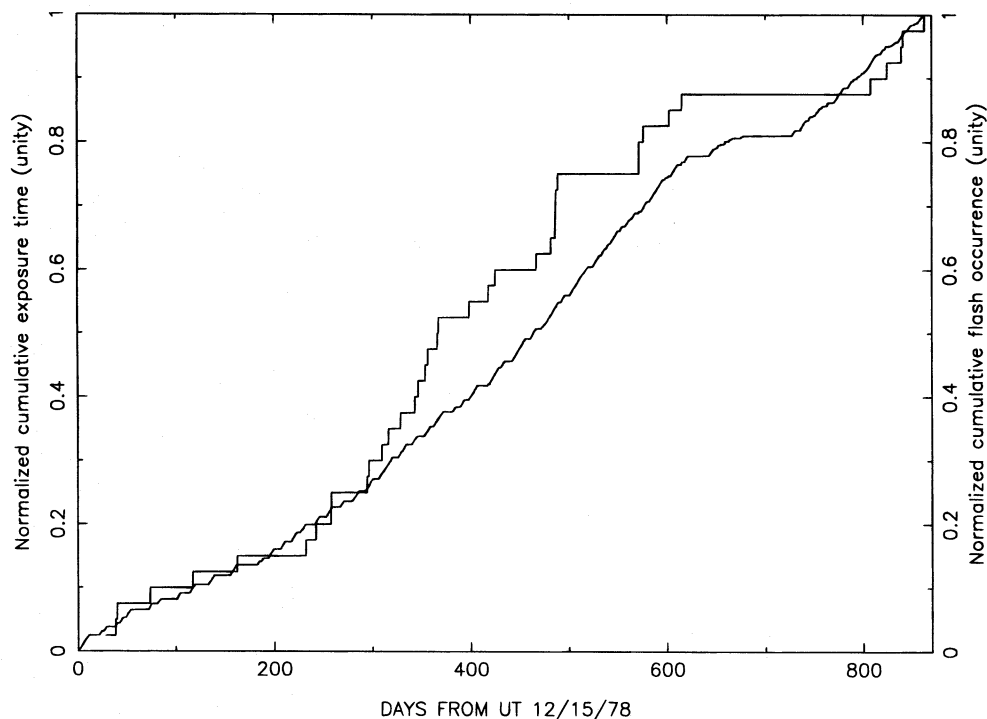

Fig. 10.—Graphical representation of the K-S test for flash occurrence time. We see no evidence that the flashes do not occur randomly with respect to the time in the mission.
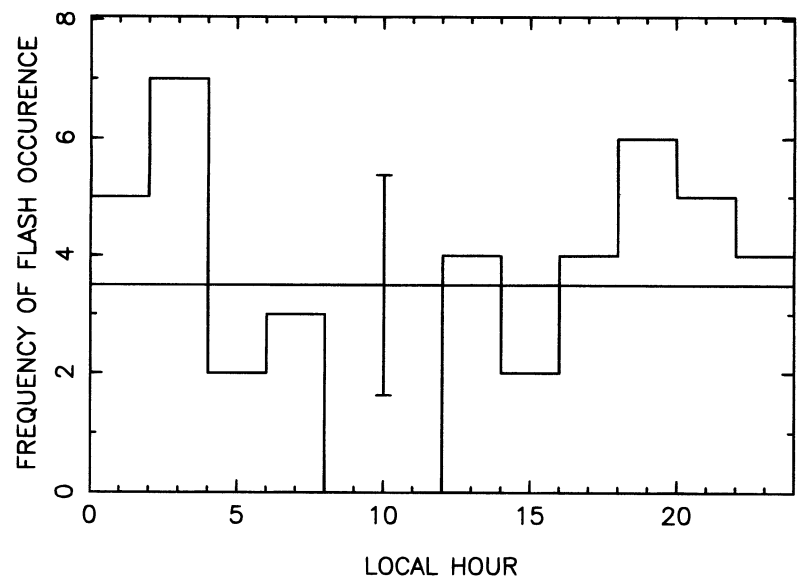
FIG. 11.—A histogram of the number of flashes binned by local solar time shows no statistically significant evidence for dependence of flash occurrence on local time. If the flashes were associated with meteoritic infall, they should occur more frequently when the satellite is over the leading hemisphere of the Earth, i.e., when local time is 0–12. Actually, an insignificant increase is detected when the satellite is in the lee of the Earth's movement through the interplanetary medium.
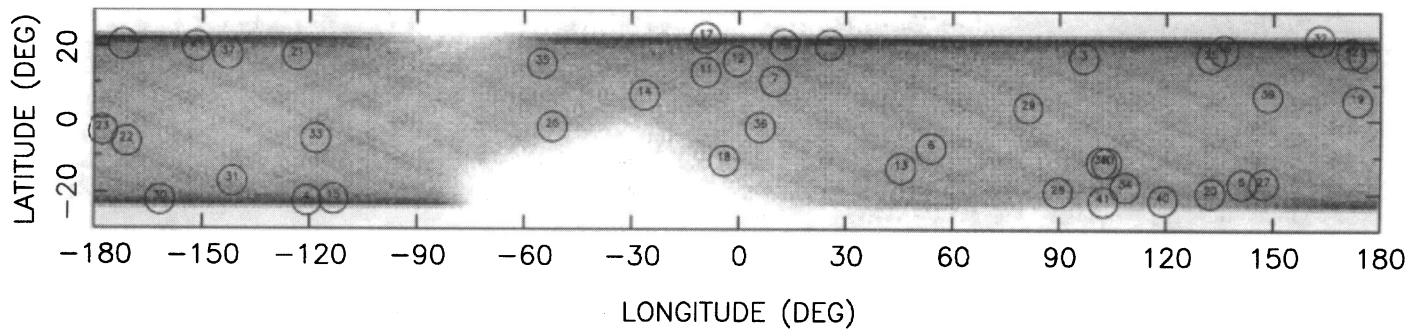

FIG. 12.—Location of the *Einstein* satellite over the Earth at the time of flash detections is indicated by the open circles. The gray-scale map represents the relative exposure time at that point over the Earth. The underexposed area around −50° is the location of the South Atlantic Anomaly. The IPC was turned off when the satellite passed through that region.

APPENDIX B

IPC DATA SELECTION CRITERIA

The Columbia IPC database (Helfand et al. 1996) allows the user to tune data selection based on the background levels, energy ranges, aspect quality, and other instrumental and environmental factors most appropriate for the task at hand. The 11 TGR criteria used to accept or reject data are displayed in Table 2, along with the range of values allowed and the specific criteria for the transient search reported here.

TABLE 2

STANDARD IPC TGR CRITERIA

TGR Criteria	Value Range	Search Settings
Background level	0–4	0–2
Viewing geometry..........	1–5	1–3
High-voltage value.........	0–9	4–9
Aspect separation	0–15	0–15
Aspect solution:		
No-aspect mode	On/off/both	Off
Lock-on mode	On/off/both	On
Extrapolated mode......	On/off/both	Off
Mapping mode	On/off/both	On
Telemetry quality	Good/bad/both	Good
Data quality	Good/bad/both	Good
High voltage................	On/off/both	On
Filter status.................	In/out/both	Out
Calibration mode	On/off/both	Off
PI bin	0–15	2–10

X PIXELS

FIG. 14

Y PIXELS

X PIXELS

FIG. 13

Y PIXELS
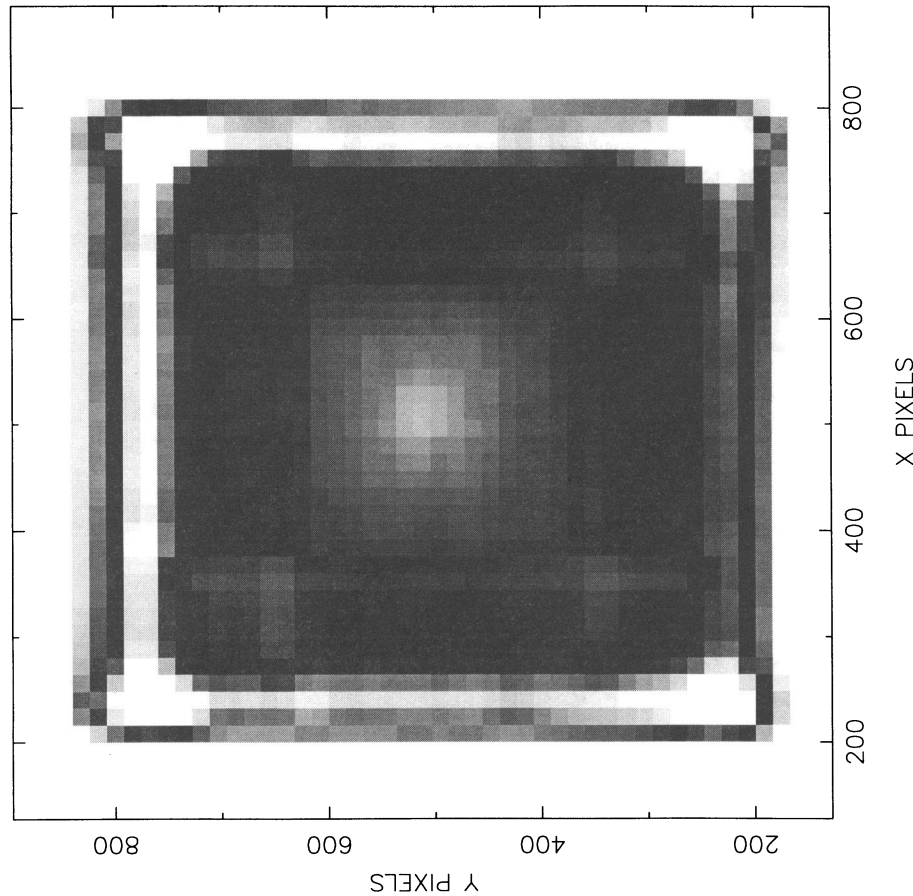
FIG. 13.—Gray-scale representation of the total amount of time the IPC was sensitive to flashes meeting our search criteria as a function of flash position in detector coordinates. Note that there is a minimum in the exposure time at the center of the detector, where we are unable to search for faint flashes because of the typical placement of strong X-ray sources there. The highest regions of sensitivity correspond to the area just outside the detector window support ribs.
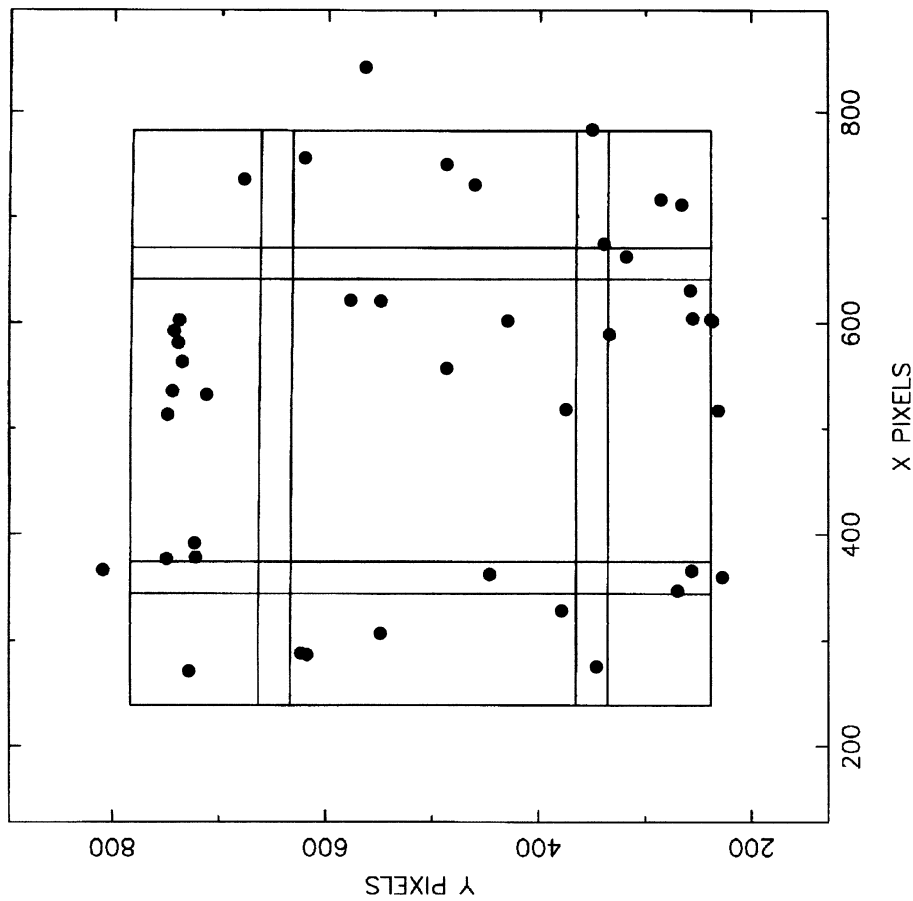
FIG. 14.—Location of flash events over the face of the IPC detector. This plot corresponds to the exposure map in Fig. 5. The lines delineate the location of the detector window support ribs. The outer box encloses the region of the IPC for which a reliable aspect solution was computed. The flashes are disproportionately concentrated toward the edge of the detector and away from the ribs, qualitatively consistent with the exposure map.

REFERENCES

Brown, T., Córdova, F., Ciardullo, R., Thompson, R., & Bond, H. 1994, ApJ, 422, 118
Fink, H. H., Schmitt, J. H. M. M., & Harnden, F. R., Jr. 1988, A&A, 193, 345
Giacconi, R., et al. 1979, ApJ, 230, 540
Gorenstein, P., Harnden, F. R., Jr., & Fabricant, D. 1981, IEEE Trans. Nucl. Sci., NS-28, 869
Gotthelf, E. V. 1992, Ph.D. thesis, Columbia Univ.
Greiner, J., Hasinger, G., & Kahabka, P. 1991, A&A, 246, 17
Hamilton, T. T., Gotthelf, E. V., & Helfand, D. J. 1996, ApJ, 466, 795
Hamilton, T. T., & Helfand, D. J. 1991, ApJ, 318, 93
Harnden, F. R., Jr., et al. 1984, SAO Report, 393
Harris, D. E., & Irwin, D., eds. 1984, The *Einstein Observatory* Revised User's Manual
Helfand, D. J., Tomaney, A., Hamilton, T. T., & Moran, E. C. 1996, in preparation
Helfand, D. J., & Vrtilek, S. 1983, Nature, 304, 41
Higdon, J. C., & Lingenfelter, R. E. 1984, in High Energy Transients in Astrophysics, ed. S. E. Woosley (New York: AIP), 568
———. 1990, ARA&A, 28, 401
Hones, E. W., & Higbie, P. R. 1989, Science, 244, 441
Iwan, D., Shafer, R. A., Marshall, F. E., Boldt, E. A., Mushotzky, R. F., & Stottlemyer, A. 1982, ApJ, 260, 111

Koyama, K., Makishima, Tanaka, Y., & Tsunemi, H. 1986, PASJ, 38, 121
Laros, J. G., Evans, W. D., Fenimore, E. E., Klebesadel, R. W., Shulman, S., & Fritz, G. 1984, ApJ, 286, 681
Lund, N., Brandt, S., & Castro-Tirado, A. J. 1991, in Proc. Workshop Univ. Alabama, Huntsville, A93-40051, 16-93, 53
Mazets, E. P., & Golenetskii, S. V. 1987, Astronomia, 32, 16
Meegan, C. A. 1994, status report available from gronews@grossc.gsfc.nasa.gov
McCammon, D., Burrows, D. N., Sanders, W. T., & Kraushaar, W. L. 1983, ApJ, 269, 107
Murakami, T., Inoue, H., Nishimura, J., van Paradijs, J., & Fenimore, E. E. 1991, Nature, 350, 592
Murakami, T., Tanaka, Y., Kulkarni, S. R., Ogasaka, Y., Sonobe, T., Ogawara, Y., Aoki, T., & Yoshida, A. 1994, Nature, 368, 127
O'Neill, T. J., et al. 1989, Science, 244, 441
Rieger, E., et al. 1989, Science, 244, 441
Share, G. H., et al. 1989, Science, 244, 441
Snowden, S., McCammon, D., Burrows, D. N., Mendenhall, J. A. 1994, ApJ, 424, 714
Wang, Q., Hamilton, T. T., Helfand, D. J., & Wu, X. 1991, ApJ, 374, 475
Wu, X., Hamilton, T. T., Helfand, D. J., & Wang, Q. 1991, ApJ, 379, 564
Yoshida, A., Murakami, T., Itoh, M., Nishimura, J., & Tsuchiya, T. 1989, PASJ, 41, 509